

## Article

# Atmospheric Circulation Drivers of Extreme High Water Level Events at Foggy Island Bay, Alaska

Peter A. Bieniek<sup>1,\*</sup>, Li Erikson<sup>2</sup>  and Jeremy Kasper<sup>3</sup> <sup>1</sup> International Arctic Research Center, University of Alaska Fairbanks, Fairbanks, AK 99775, USA<sup>2</sup> U.S. Geological Survey, Pacific Coastal and Marine Science Center, Santa Cruz, CA 95060, USA<sup>3</sup> Alaska Center for Energy and Power, University of Alaska Fairbanks, Fairbanks, AK 99775, USA

\* Correspondence: pbieniek@alaska.edu; Tel.: +1-(907)-474-5813

**Abstract:** The northern coast of Alaska is experiencing significant climatic change enhancing hazards from reduced sea ice and increased coastal erosion. This same region is home to offshore oil/gas activities. Foggy Island Bay is one region along the Beaufort Sea coast with planned offshore oil/gas development that will need to account for the changing climate. High water levels impact infrastructure through coastal erosion and flooding hazards. In this study, 21 high water level events exceeding the top 95th percentile were identified at the gauge in Prudhoe Bay, Alaska (adjacent to Foggy Island Bay) over 1990–2018. All 21 events, and many non-extreme days with elevated water levels, were associated with strong westerly winds according to station records. Storm systems were generally found to be a key driver of westerly winds in the region according to downscaled reanalysis and storm track data. A dynamically downscaled global climate model projection from CMIP5 indicated that days with westerly wind events may become more frequent as storms strengthen and have longer durations by 2100 in the Foggy Island Bay region. Coupled with the anticipated continued decline in sea ice, the northern coast of Alaska may experience more frequent high water events over the next ~80 years.

**Keywords:** Arctic storms; coastal flooding; climate change



**Citation:** Bieniek, P.A.; Erikson, L.; Kasper, J. Atmospheric Circulation Drivers of Extreme High Water Level Events at Foggy Island Bay, Alaska. *Atmosphere* **2022**, *13*, 1791. <https://doi.org/10.3390/atmos13111791>

Academic Editor: Alexey V. Eliseev

Received: 27 September 2022

Accepted: 27 October 2022

Published: 29 October 2022

**Publisher's Note:** MDPI stays neutral with regard to jurisdictional claims in published maps and institutional affiliations.



**Copyright:** © 2022 by the authors. Licensee MDPI, Basel, Switzerland. This article is an open access article distributed under the terms and conditions of the Creative Commons Attribution (CC BY) license (<https://creativecommons.org/licenses/by/4.0/>).

## 1. Introduction

The Arctic contains significant oil and gas resources [1] that are being considered for or are undergoing commercial development. Climate change in the Arctic may benefit these development opportunities but also bring challenges. These challenges include impacts from changing storminess, coastal erosion, and melting permafrost. The planning for potential offshore oil and gas development in Foggy Island Bay (located in Stefansson Sound), Alaska (see Figure 1) is facing these competing forces from climate change. Here, as is the case throughout the Arctic, the climate is warming faster than in lower latitudes [2,3] and is projected to continue to warm in the coming decades. The placement of on-shore infrastructure to support the offshore island is potentially vulnerable to coastal erosion and flooding from storms. Storms that cause such flooding events are common in coastal areas of Alaska [4,5]. Understanding the role and possible future conditions of these storms in the Foggy Island Bay region is important to safely plan for future commercial development.

Communities along the Beaufort Sea coast of Alaska are vulnerable to coastal flooding [6]. The occurrence of high wave events, storm surges, and coastal flooding is tied to the strength and direction of the winds. In Alaska, the largest storm surges are associated with strong southwesterly winds due to extratropical cyclones in the Bering Sea impacting the west coast of Alaska [4] while strong winds over 13 m/s were found to be a key driver of similar events at Utqiagvik [7]. Strong westerly winds have been reported to occur in conjunction with historical storm surge events/high water levels along the Beaufort Sea coast in the vicinity of Foggy Island Bay [8–10]. The presence of sea ice and landfast ice that

reduce or eliminate the fetch during much of the year strongly influence the surge levels, and although significant water level fluctuations occur beneath the sea ice, coastal impacts from overland flooding is reduced by the impeding ice cover [7,11].

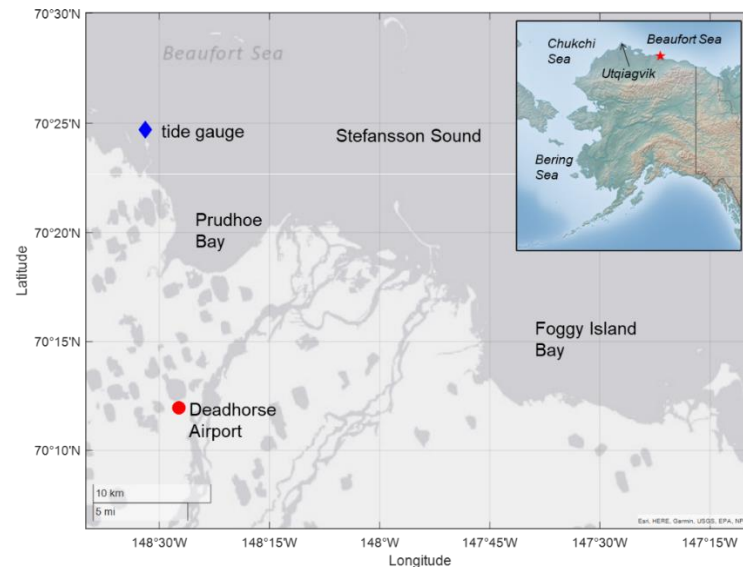


**Figure 1.** Map showing the Foggy Island Bay focus region along with the locations of the tide gauge (blue diamond) in Prudhoe Bay and the Deadhorse Airport weather station (red dot). The star in the inset map shows the location of the study region in northern Alaska.

Near-surface winds in the vicinity of Foggy Island Bay and adjacent Prudhoe Bay are predominantly easterly [12]. These easterly winds generally occur under the influence of the Beaufort High centered to the north [13,14]. During the summer months sea breezes also form in the area [15–19]. In northern Alaska, coastal flooding from storm surges is often associated with westerly wind events [9]. Westerly winds in the region occur when a storm system is centered over the Beaufort Sea and increased cyclone activity there is correlated with a weaker Beaufort High [20].

There is some uncertainty in the historical trends of winds and storms in northern Alaska. Historically, mean and 95th percentile wind speeds have increased since 1979 along the Beaufort Sea coast according to reanalysis data [21] although there are mixed trends in station data [22]. Historical trends in storm tracks generally do not show coherent signals but there is evidence that strong or extreme storms are becoming more frequent in the Arctic Basin, especially in winter [23,24]. For the Foggy Island Bay region, enhanced storminess is corroborated by a trend toward a weakened Beaufort High [20] and recent years that experienced a “collapse” of the same feature [25,26]. Beyond the atmospheric circulation parameters, Arctic sea ice extent has displayed a notable decline over the satellite record providing more fetch for wave/surge development. In northern Alaska, the frequency of high wind events is anticipated to increase especially during the fall and winter [27,28], which, coupled with declining sea ice, may be a recipe for more frequent high water events.

The economic importance of the Foggy Island Bay study area, uncertain regional climatic trends in winds/storms over the observational record, and its vulnerability to coastal flooding impacts make understanding the drivers, and potential changes, of such events important for planning. The primary objectives of this study are to (1) link historical high-water events with atmospheric drivers; and (2) develop future projections for how such wind or storm events might change. While tides and sea level rise are also important factors in determining historical and future coastal water levels, this study primarily focuses on the atmospheric drivers.

## 2. Materials and Methods

Historical and future projections of gridded hourly meteorological variables of wind, temperature, and sea level pressure were obtained from the Scenarios Network for Alaska and Arctic Planning and are available online at <https://registry.opendata.aws/wrf-alaska-snap/> (accessed on 1 August 2018). These are an hourly, 20 km spatial resolution dynamically downscaled data set covering all of Alaska and adjacent land and ocean areas based on the ERA-Interim Reanalysis (1979–2015). Similarly downscaled future projections over 1970–2100 from the Geophysical Fluid Dynamics Laboratory Coupled Physical Model, version 3 (GFDL) and National Center for Atmospheric Research Community Climate System Model, version 4 (CCSM) were also obtained. The downscaled GFDL and CCSM models include a historical simulation (1970–2005) and RCP 8.5 scenario (2006–2100); however, this study is focused on the 1979–2100 period. These two global climate models were downscaled because they provided the best simulations of temperature, precipitation, and sea level pressure for the Alaska region based on an evaluation of Coupled Model Intercomparison Project, phase 5 models [29]. All three data products described above were downscaled using the Weather Research and Forecasting (WRF) model [30] within a domain that spanned all of Alaska and adjacent areas of Canada, Russia, and the Arctic Ocean [31–33]. For the dynamical downscaling procedure, WRF utilized the Morrison 2-moment microphysics [34] and the Grell 3D cumulus scheme, while radiative effects were parameterized by the Rapid Radiative Transfer Model (RRTM) for GCMs [35]. The boundary layer was modeled via the Mellor-Yamada-Janjic scheme [36], while Janjic eta was used for surface processes. The full description of the physics packages, domain and model setup are described in Bieniek et al. [31]. Sea ice concentrations were prescribed in the WRF downscaling simulations and were directly interpolated to the 20 km grid from the input ERA-Interim, GFDL and CCSM data sets. Therefore, the sea ice concentrations available with the downscaled data were used in our analysis for ease of comparison with the other downscaled meteorological variables. Sea ice was assessed in a limited area in the vicinity of Foggy Island Bay within a 69.5–73° N latitude and 142–152° W longitude box (see Figure 2a).

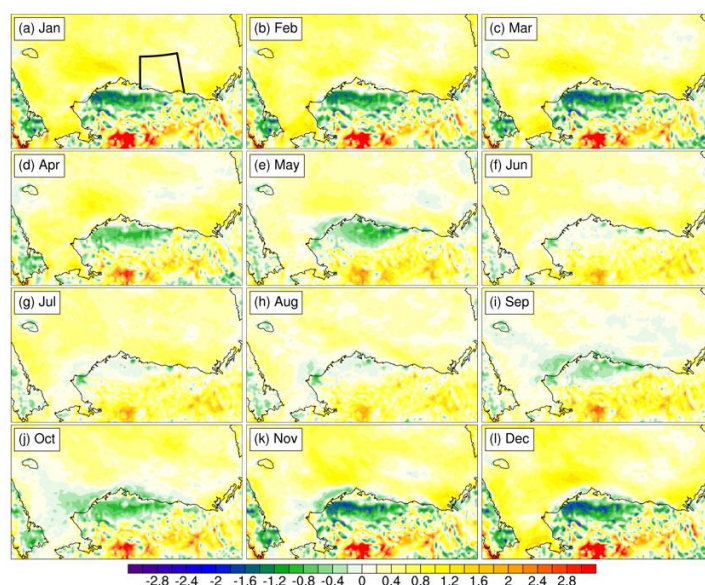


**Figure 2.** Monthly difference downscaled ERA-Interim minus CBHAR of daily 90th percentile wind speed threshold for 1979–2009. The month is displayed in each panel and units are m/s. The region of the sea ice analysis is outlined by the box in (a).

Storm activity and tracks were quantified and evaluated using the National Centers for Environmental Prediction–National Center for Atmospheric Research Reanalysis 1 (R1) to capture a larger domain than was available in the high-resolution downscaled data

described above. Individual cyclones were identified and tracked through time using the storm tracking algorithm described by Zhang et al. [37] on the R1 6-hourly gridded sea level pressure fields at 2.5° spatial resolution. The storm tracking algorithm was also applied to the downscaled ERA-Interim, GFDL and CCSM after interpolation to the same spatial and temporal resolution as R1 for comparison.

Due to the lack of station data in the region additional validation of the downscaled winds was conducted against the higher spatial resolution and more temporally limited 1979–2009 historical data from the Chukchi-Beaufort High-Resolution Atmospheric Reanalysis (CBHAR), which is available online at <https://portal.aos.org/> (accessed on 10 August 2018). Like the 20 km downscaled data described above, CBHAR was also produced using WRF driven by ERA-Interim, but it also included additional data assimilation from station and satellite data sources [38]. These data were able to more accurately capture many nuances of the wind field in the region [39] making them an excellent data source for validation purposes.

The CBHAR and 20km downscaled ERA-Interim data compare favorably for daily 90th percentile threshold wind speeds for each month in the overlapping 1979–2009 period (Figure 2). Similar results were found in overall long-term monthly means (not shown). Larger discrepancies primarily occur farther inland from the coast. This study utilized a bias-corrected station wind product based on the 20 km dynamically downscaled data available online at <http://windtool.accap.uaf.edu/> (accessed 15 September 2020) for analysis of weather station winds. These corrected hourly wind speed data were produced via quantile mapping adjustments to quality controlled station data [27]. This study used these daily bias-corrected data for the Deadhorse Airport unless otherwise explicitly noted.

Water level and meteorological data were obtained from the nearest tide gauge station located at Prudhoe Bay (<https://tidesandcurrents.noaa.gov/stationhome.html?id=9497645>; accessed on 1 February 2019), which is less than 30 km west of Foggy Island Bay. Winds were obtained from the tide station but were not measured at a standard 10 m height and are therefore only presented for limited cases when explicitly noted. Additional hourly meteorological data from the Deadhorse Airport (also located near Prudhoe Bay), was obtained from <https://mesonet.agron.iastate.edu/request/download.phtml> (accessed on 15 September 2020), and was used only when hourly data was needed for validation purposes of the downscaled wind data described above.

Analysis of the data was conducted via standard statistical methods including the Pearson correlation coefficient. Trends were assessed using the Theil-Sen estimator approach and the significance was evaluated using the Mann–Kendall trend test. A simple map clustering approach using pattern correlation [40] was employed to objectively group similar sea level pressure patterns.

### 3. Results

#### 3.1. Local Impacts of Wind Events

The historical frequency of observed daily maximum water levels were compared with mean daily wind direction observed at Deadhorse and are shown in Figure 3a. The windrose computed for the Deadhorse Airport station based on hourly data (Figure 3d) shows that winds are most frequently from the east and northeast with a smaller secondary peak from the west. Winds during the highest water level event bins in Figure 3a are predominantly from a westerly direction. Conversely, lower water levels are often associated with easterly winds, although there are instances of westerly winds as well. Wind speeds recorded at Deadhorse during high and low water levels were generally more mixed (Figure 3b) with stronger and weaker winds occurring more evenly across the distribution than wind direction.

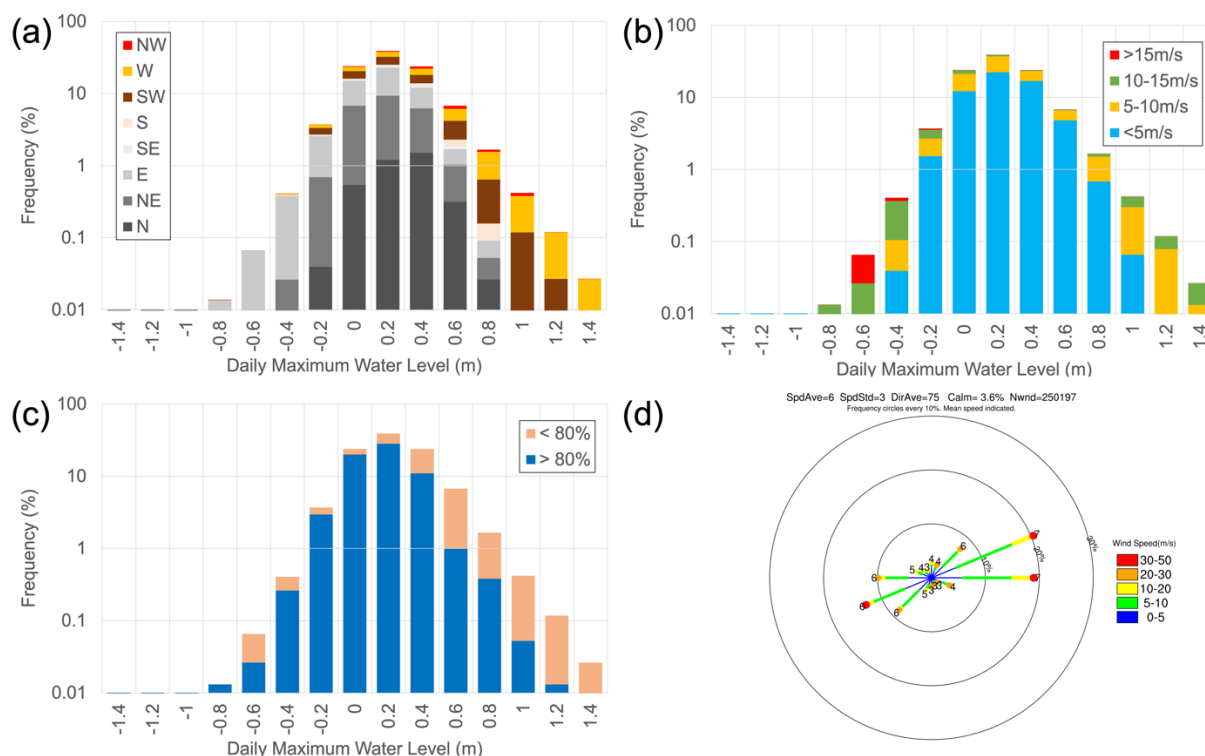


**Figure 3.** Histograms of the historical frequency of daily maximum water level subdivided by the associated (a) daily mean wind direction; (b) daily mean wind speed; and (c) daily mean sea ice concentration. The *y*-axis is on a logarithmic scale to highlight the extreme tails of the distribution. Windrose of the frequency of hourly station wind speed and direction from the Deadhorse Airport for 1979–2009 is shown in (d).

The 21 days with the highest water levels exceeding the 95th percentile were ranked (Table 1). These highest water level events all occurred under westerly wind conditions according to the wind data collected at the tide gauge. This is also reflected by the analysis of all daily wind and water level conditions presented in Figure 3a as events with the highest water levels all occurred under westerly wind regimes while the lowest water levels occurred during easterly winds. There were 38 days with mean wind speeds exceeding 15 m/s during the period analyzed. Only four days with winds in this highest category occurred under westerly wind conditions while the rest were under easterly winds. Most of the highest water levels occurred on days when daily average winds fell in the more common 10–15 m/s range. The daily maximum wind speeds for the 95th percentile water level events fell within a range of 12.7–22.3 m/s at the location of the tide gauge. According to the hourly station wind data at Deadhorse, strong winds exceeding 20 m/s occur most frequently under easterly winds (Figure 3b).

Fetch due to open water is a key factor for high water events under high winds. The average ice concentrations in the waters bounded to the south by the coast, to the north at 73° N, and east–west 152–142° E, were derived from the downscaled ERA-Interim reanalysis. The sea ice is an interpolation to the 20 km downscaled grid as the surface boundary forcing field in the WRF model [31] and comes from the passive microwave products ingested into the original ERA-Interim reanalysis [41]. These “downscaled” sea ice fields were used for consistency with the downscaled global climate model data that will be presented later in this section. The daily mean sea ice concentrations below an arbitrary threshold of 80% within the box described above were aligned with the observed water levels (Figure 3c). The days with the highest water levels tended to occur when ice concentrations were lower than 80%. However, there were multiple days during the winter

months when relatively high water levels were measured and sea ice concentrations were greater than 90%.

**Table 1.** Water level (m) extremes exceeding the daily 95th percentile with maximum daily wind speed (m/s) and mean wind direction (degrees) from the tide gauge station at Prudhoe Bay (1990–2017). Minimum storm central pressure (hPa) and total duration of the storm (h) impacting the region identified by the storm tracking algorithm using R1 are also shown. Water levels include storm surges, astronomic tides, and seasonal water level variations.

Date	Water Level	Wind Speed	Wind Direction	Storm Central Pressure	Storm Duration
11 August 2000	1.37	17.8	271	993.4	48
30 July 2003	1.26	22.1	285	975.9	42
9 October 2002	1.15			983.3	120
31 July 2008	1.12	18.8	251	982.6	72
15 August 2002	1.12	20.8	290	979.8	36
26 February 2011	1.05	17.6	269	977.1	12
5 August 2003	1.04	16.6	291	987.5	36
18 July 2016	1.02	23.9	262	990.5	78
11 November 2013	1.00	15.3	242	971.1	54
30 September 1994	1.00	16.0	233	1003.1	228
31 July 2004	0.98			998.9	30
1 September 2018	0.98			985.1	18
5 January 2017	0.96	17.5	252	992.4	60
6 October 2002	0.94	19.8	257	984.0	54
19 September 2016	0.94	12.7	277	982.4	108
16 August 1997	0.93	18.9	276	988.6	12
6 January 2004	0.91	22.3	243	1002.0	30
18 August 1994	0.89			976.9	36
16 December 2008	0.88	12.2	183	999.1	42
25 July 2003	0.87	18.1	235	983.3	72
25 July 2017	0.87			996.7	48

The extreme events primarily occurred during Jul–Oct but a few events occurred during the winter months (Table 1) when the presence of sea ice can impede the formation of high water levels. The seasonality of all westerly wind events and antecedent wind speed and ice conditions are shown in Figure 4. Historically, most westerly wind events occur in Dec–Jan with a minimum in Jun–Jul (Figure 4a) and is reflected in both the downscaled reanalysis and station observations. The average wind speeds associated with westerly wind events is similar throughout the year ranging from 4 to 5 m/s (Figure 4b). Regional sea ice concentrations during westerly wind events are high in most months except during the summer and fall (Figure 4c). The two downscaled climate model projections in our analysis both indicated increased frequencies of westerly wind events starting in the fall and extending into early winter and declines or no trends later in the winter and summer over 2015–2100. The wind speeds during these events are projected to increase, especially in Nov–Jan in GFDL. Sea ice concentrations during westerly wind events are anticipated to decline throughout the year with changes of around 100% (i.e., full open water) in summer, fall and early winter.

The overall decadal average number of westerly wind events per year near Foggy Island Bay spanning the historical and future projections is shown in Figure 5. During the historical 1980–2010 period, the station observations and downscaled reanalysis correspond well, although the station tended to have more events than the downscaled reanalysis. The station had approximately 160 days with westerly winds per year in the 1990s and 2010s and the 2000s was the lowest decade with 149 days per year. The 2000s minimum was more pronounced in the reanalysis than in the station data. The projections diverge with CCSM showing flat or even declines while GFDL had an increased number of days with westerly winds, especially starting in the 2060s. For GFDL the mean number of days per year was

161 in 2010–2050 and increased to 173 in 2060–2100. For CCSM, the mean number of days per year was 152 in 2010–2050 and declined to 147. These changes reflect a projected 7% increase and 3% decrease in the annual frequency of days with westerly winds between the two periods in GFDL and CCSM, respectively.

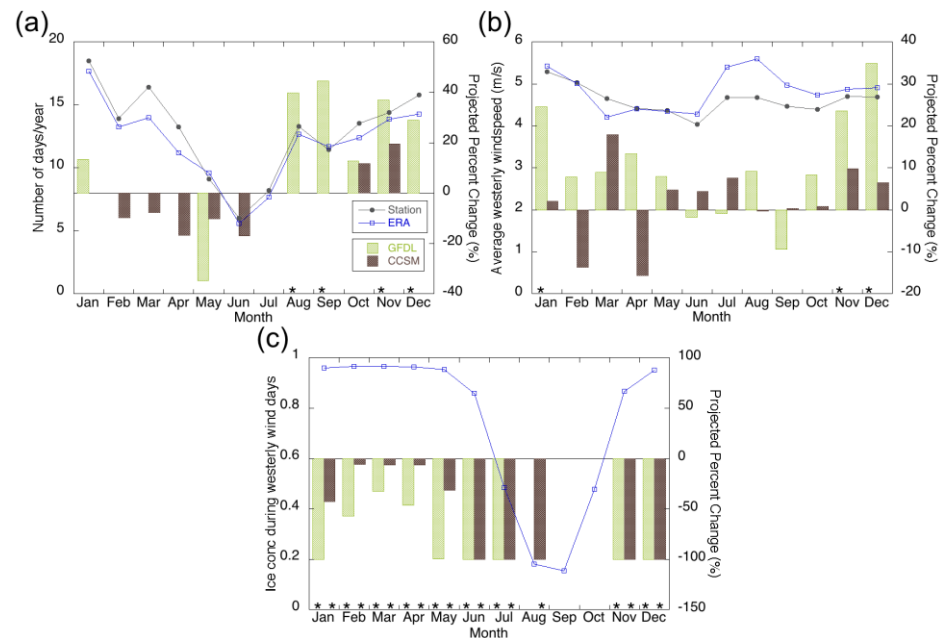


**Figure 4.** Monthly historical climatology (1991–2010; lines) and projected percent change over 2015–2100 (bars) for the (a) number of days with westerly winds, (b) average wind speed on days with westerly winds, and (c) daily average sea ice concentration during westerly wind days. Trends significant at the 95% or greater level are marked with an asterisk along the x-axis.

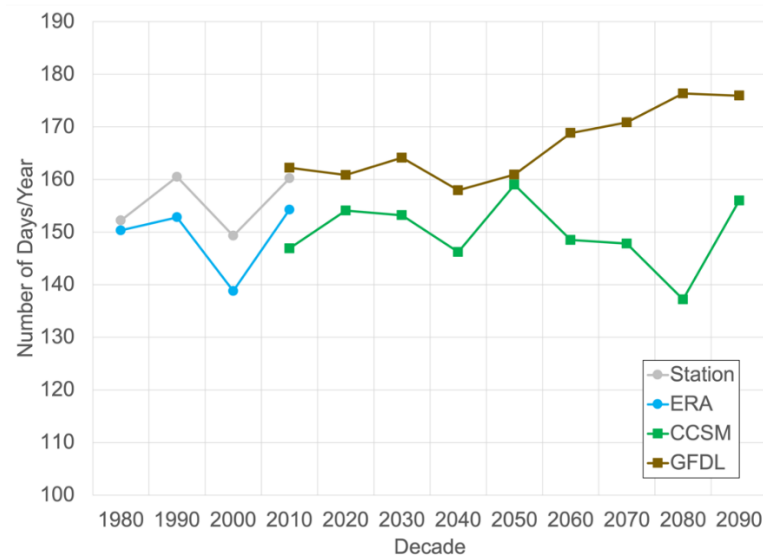


**Figure 5.** Historical and projected decadal average counts of days with westerly winds. Units are days per year. The decadal average counts of events in the CCSM and GFDL projections were delta bias-corrected using the historical mean difference from the observations.

### 3.2. Large-Scale Atmospheric Drivers

The daily sea level pressure patterns, wind speeds, and wind vectors associated with the extreme events in Table 1 are shown in Figure 6. All days feature a low pressure system centered over the Beaufort Sea. Two general pressure patterns emerged based on the map

typing analysis. The most common were days with storms centered directly north of the study area. This placement of the cyclone generally brings westerly or west-northwest winds into Foggy Island Bay. A secondary pattern with storms centered farther east was present on a few of the days and also brought westerly winds to the region. There was a broad range of daily mean wind speeds according to the downscaled reanalysis on these days with some exceeding 14–15 m/s and others with much weaker winds. However, rapidly evolving storm conditions that lasted a short duration during the day may have been washed out in the daily means. The location of the storm centers was accurately captured by the independent storm tracking algorithm and the multiple centers reflect the 6-h time step of the algorithm and underlying data.

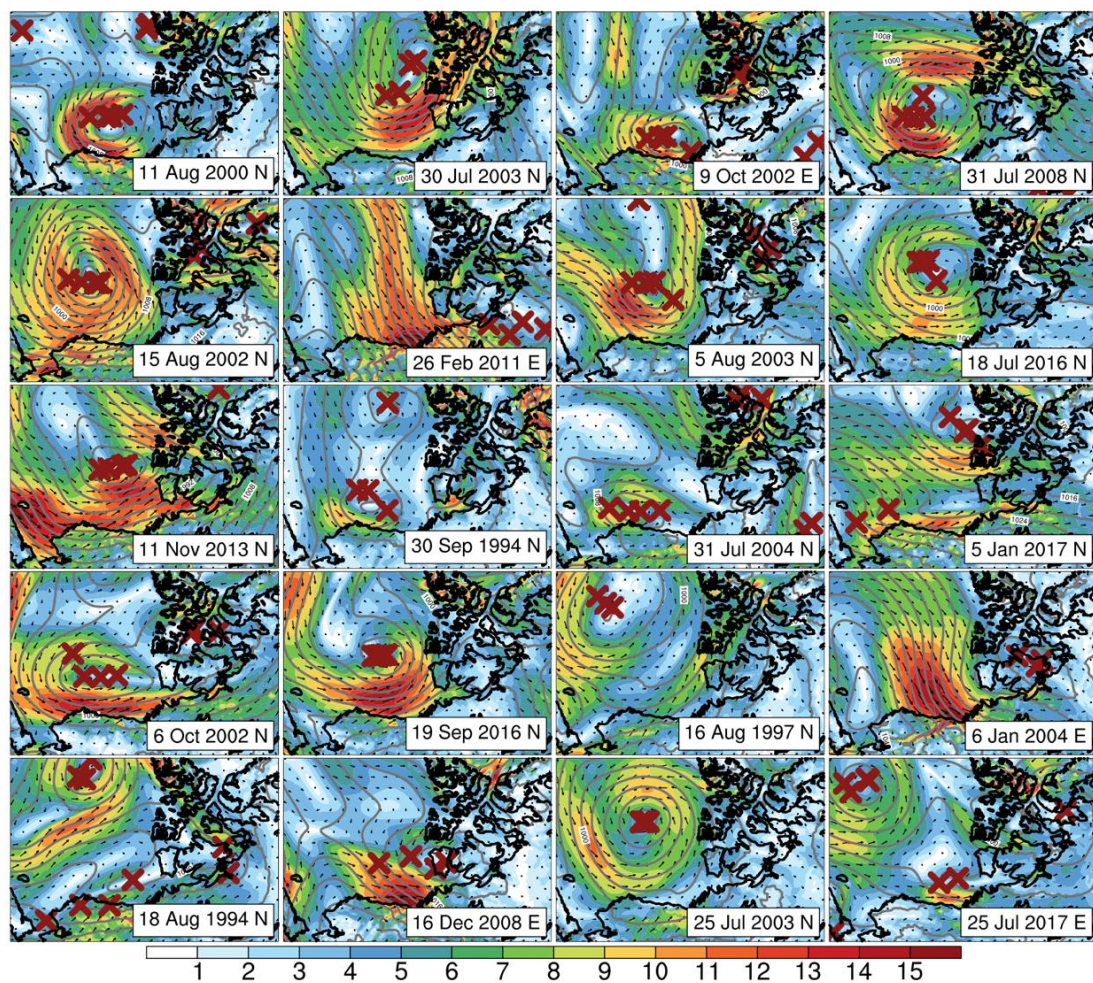


**Figure 6.** Sea level pressures (gray contour lines), wind speeds (m/s, shading), wind vectors, and the locations of storm centers (red X) for the days with extreme high water levels listed in Table 1. The 25 July 2017 event is not shown as it was outside of the available date range of the downscaled ERA-Interim. The map classification (N—north; E—east) is shown along with the date in the label on each panel.

At the annual scale, higher numbers of storms tracking into the Foggy Island Bay region (see blue box in Figure 7) were associated with more frequent elevated water levels >0 m (correlation 0.62 annual storm counts vs. annual water level frequencies). Annually, storms with deeper central pressures and longer durations were also correlated with more frequently elevated water levels (correlations −0.47 and 0.30, respectively). Likewise, more frequent, stronger, and longer duration storms were annually associated with more frequent westerly winds and stronger wind events. At the daily scale, 73% of days that had a storm identified in the region had concurrent westerly winds at Foggy Island Bay during

the historical period (storms with centers located on the far edges of the box may have more limited influence). The origins of the individual storms that tracked into the Beaufort Sea region on the 21 days with highest water levels were quite variable and are shown in Figure 7. There were 28 storms associated with the extreme days according to the storm tracking algorithm that intersected with the region. Many storms (~12) formed locally, and nearly two thirds of all the storms counted formed within the Arctic. Some of the local storm generation may be due to storm systems that tracked longer distances but split while transiting into the region. Most storms that tracked from outside of the Beaufort Sea region formed along the Siberian coast while a few (i.e., 3–5) storms tracked from northern Japan and Asia. However, there was no coherent pattern in the origin of the storms that led to the high water events. Generally the storms associated with the 21 extreme events were within the Foggy Island Bay region for 58.9 h on average (Table 1). However, the durations ranged from as little as 12 h to over 100 h in a few instances. There was a slight positive correlation (0.25) between the minimum central pressure and duration of the storms for the extreme events. This indicates that storms with weaker (i.e., higher) central pressures tended to be in the region longer prior to the extreme events than stronger storms.

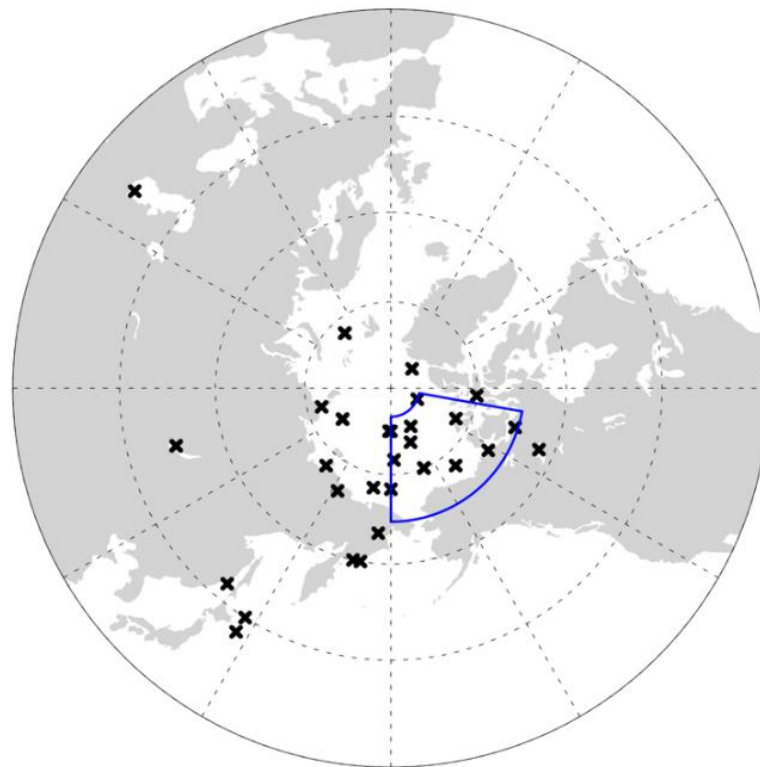


**Figure 7.** Origin locations of cyclones identified based on the R1 sea level pressure data in the region on days with extreme high levels listed in Table 1. The blue box denotes the region in which storms needed to be located at least once during each day to be included.

When all daily water levels were correlated more broadly with sea level pressure a negative correlation was found with its maximum ( $\sim -0.5$ ) centered over the Beaufort Sea (Figure 8a). Relatively weak positive correlations ( $\sim 0.18$ ) with daily water level are also found farther south in the Gulf of Alaska and southern Bering Sea. This pattern of correlations indicates that lower pressures over the Beaufort Sea generally occur in conjunction with higher water levels at Prudhoe/Foggy Island Bay. The westerly component of near surface winds in the same area is similarly correlated with sea level pressure (Figure 8b). The strongest westerly winds occur under low pressure in the Beaufort Sea with high pressure over the Bering Sea.

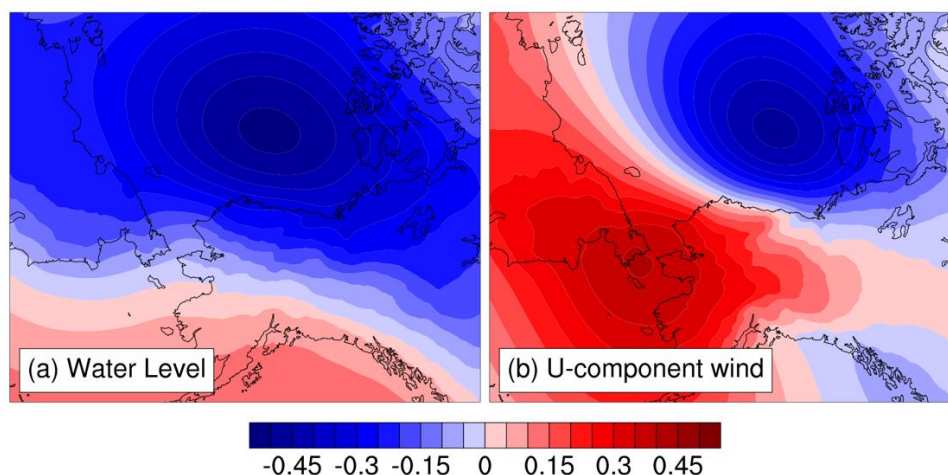


**Figure 8.** Correlation of daily mean (a) water level at Prudhoe Bay, and (b) east–west u-component of the wind at Deadhorse with the daily gridded sea level pressure for the available period of record. All correlations are significant at the 95% or greater level within the domains shown in (a,b).

Trends in seasonal historical sea level pressure (SLP) and the long-term average climatological values over 1979–2017 are shown in Figure 9a–d. The historical climatologies all exhibit the Beaufort High centered north of Alaska, to varying degrees, throughout the year. There were only limited statistically significant trends in sea level pressure in the Beaufort Sea region over the historical period. Most significant trends occurred elsewhere in the region such as over the Chukchi Sea in Sep–Nov or the Bering Sea in Mar–May. Over the Beaufort, trends were mixed over most seasons except for Sep–Nov when there were the most widespread declines on the order of  $-0.5$  hPa per year. Although not having statistical significance, such declines in pressure would be consistent with increasing storminess.

While change over the historical observational period was generally subdued, more substantial changes are anticipated as the climate warms over the 21st century. Projected changes in sea level pressure according to the two downscaled global climate models over 2015–2100 are shown in Figure 9e–l. Both projections suggest that SLP will decline in Sep–Nov and Dec–Feb over the Beaufort Sea north of Alaska (around  $-0.3$  and  $-0.8$  hPa per year in CCSM and GFDL, respectively) with mixed or weaker trends in Mar–May and Jun–Aug. The downscaled GFDL projection generally has the most significant downward trends of the two estimates. The model historical climatologies for 1979–2017 for each season are also displayed in Figure 9e–l for reference.

Related to the past and future anticipated changes in SLP described above, understanding variability and change in storm activity is important to consider possible futures for extreme water level events. As was the case with the historical westerly winds and storms described earlier in this section, the storms identified in the box outlined in Figure 7 were present on 67–81% of days with westerly winds at Foggy Island Bay in GFDL and CCSM (and was generally consistent through 2005–2100). The decadal averages of the annual counts of storms tracking into the Foggy Island Bay region has generally increased since 1979 according to the available data (Figure 10a). Little or no change in the annual frequency of storminess is anticipated in future decades according to the two downscaled global climate model projections. However, declines in the central pressure (i.e., strengthening) of the storms is anticipated by both projections by 2100 (Figure 10b). Future change is more mixed with annual average duration of storms in the Foggy Island Bay region with GFDL showing increases and CCSM having declines (Figure 10c). Increases in either the strength or durations of storms could potentially result in enhanced westerly winds and increased likelihoods of extreme high water level events.

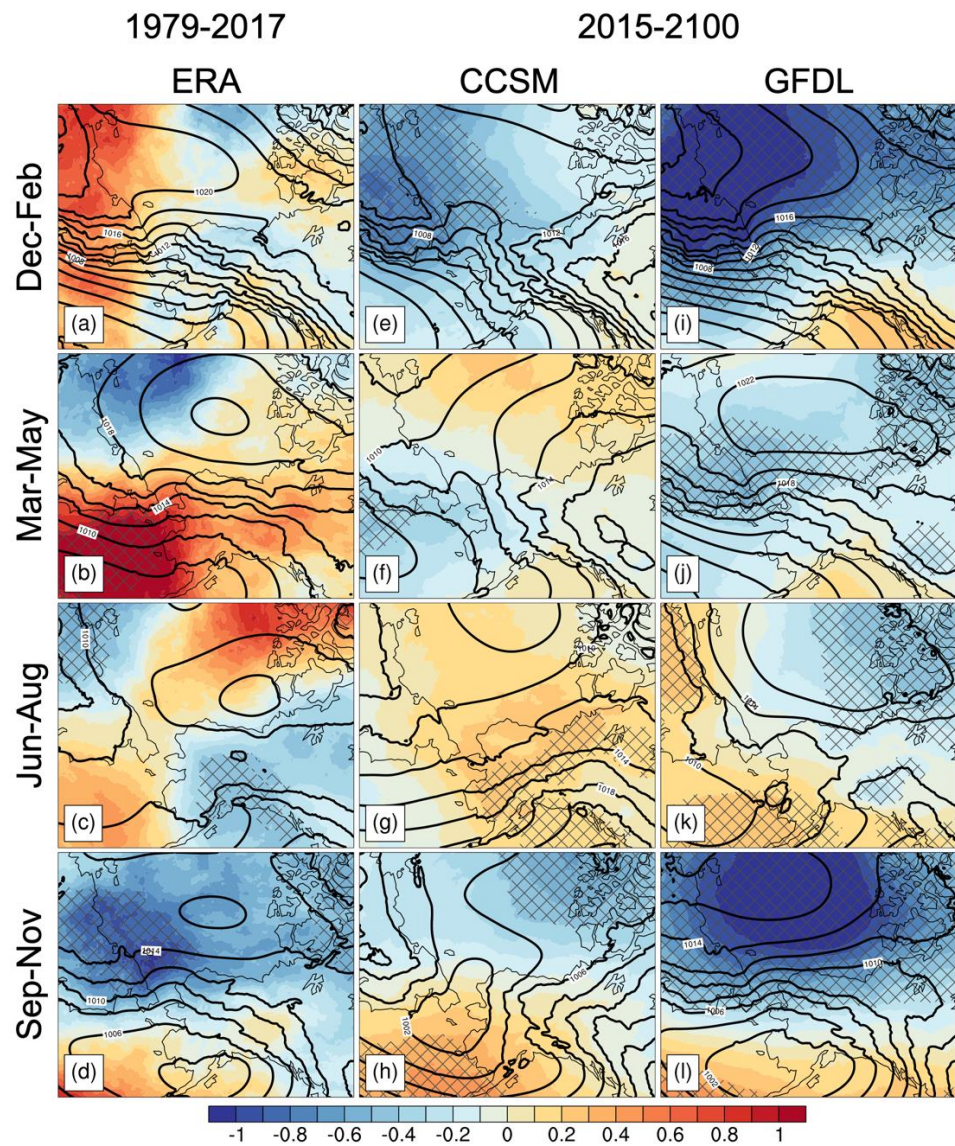


**Figure 9.** Seasonal sea level pressure trends and historical climatology for downscaled (a–d) ERA-Interim for, (e–h) CCSM, and (i–l) GFDL. Colors are sea level pressure trends (hPa/yr). Hatching denotes regions of trends significant at the 95% or greater level according to the Mann–Kendall test. Trends for ERA-Interim cover the 1979–2017 period while CCSM and GFDL are for the future 2015–2100 projection. Contours denote the historical climatologies (1979–2017) for the downscaled ERA-Interim reanalysis, CCSM and GFDL.

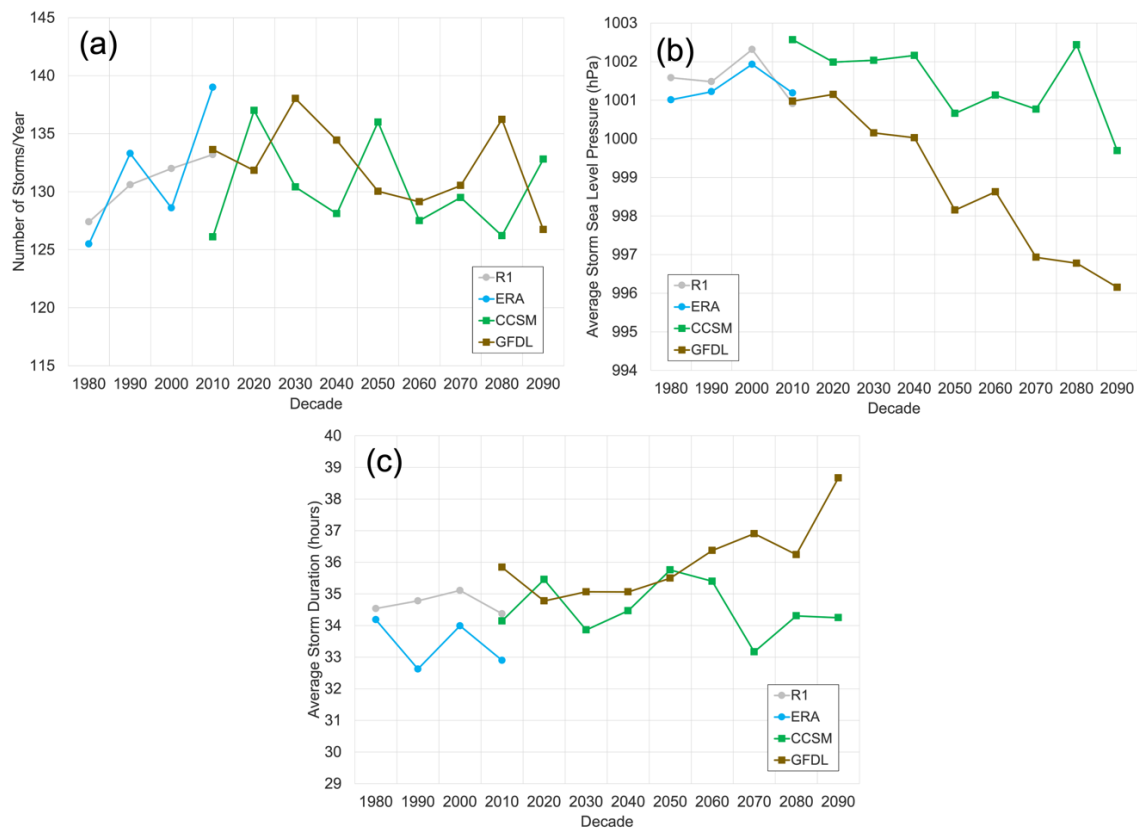


**Figure 10.** Historical and projected decadal average (a) number of storms per year, (b) central pressure of storms (hPa), and (c) storm duration (hours) for storms entering the region shown by the box in Figure 7. The decadal average counts of events in the CCSM and GFDL projections were delta bias-corrected using the historical mean difference from R1.

#### 4. Discussion

The results paint a picture of high-water events in Foggy Island Bay being linked to westerly winds that arise from the passage of storm systems, which may increase in frequency into the future under climate change. Westerly winds and high water levels were found to be negatively correlated with sea level pressure north of Alaska. This is indicative of increased westerlies being associated with enhanced storminess over the Beaufort Sea, which was confirmed by the positive correlations between water levels, westerly winds and the numbers of storms occurring in the region. Individual storms centered either to the north or east of Foggy Island Bay were also tied to individual extreme events. These results are also consistent with prior studies connecting sea level pressure patterns and high winds at the nearby Deadhorse Airport [28] and westerly wind events along the Beaufort Sea coast [9]. Many of the storms associated with the extreme high water events originated within the region, which is consistent with results of a prior analysis of storms, albeit in winter, over the Beaufort Sea [25].

While not a direct focus of this study, tides and sea states also play an important role in modulating coastal water levels. Astronomic tides in the region are small and the Prudhoe Bay tide gauge shows a total astronomic tidal range <25 cm with winds and low pressures (inverse barometer effects) accounting for the greatest water level variations. The mechanism by which winds force changes in coastal water levels is through Ekman dynamics with westerly winds along an east–west oriented coastline producing an increase or setup of coastal water levels (a surge) as well downwelling of surface waters, while easterly winds produce a lowering or setdown of the coastal water level and upwelling of deeper water to the surface (e.g., [42]). Maximum recorded setup and setdown are about equal. Furthermore, note that the coastal water level increases noted in the Prudhoe

Bay record (Table 1) are likely a combination of mode 0 (storm surge) and higher level, propagating coastal trapped wave modes (e.g., [43]) but the high correlation between local winds and water levels indicate that the primary response is due to direct wind forcing. A more detailed analysis of the contribution of the different coastal trapped wave modes is beyond the scope of the current manuscript.

The results showed that the westerly wind forcing of high water level events was correlated with storms and, more broadly, with regional sea level pressures. Historically, trends in sea level pressure across the Beaufort Sea and extending northward over the Arctic Ocean in most seasons were mixed over 1979–2017. The Sep–Nov period featured declining trends but these were generally of low significance. Annually, the number of storms increased over the historical record since 1979 in the Foggy Island Bay region. Prior studies have shown a strengthening of the Beaufort High in this region over the historical record in the summer months (e.g., [14,44]). However, recent declines in the strength of the Beaufort High have been noted in the winter [26] and annually [20]. A weakened Beaufort High allows for greater cyclone activity over the Arctic [20], which could result in more frequent or intense westerly wind events at Foggy Island Bay depending on the trajectory of the storm systems. Many of these storms originated locally or in the Arctic, which is consistent with prior analysis of storms impacting the Beaufort Sea [45] and more broadly in the Arctic [20,24,37,46]. There was a positive trend in the historical frequency of storms impacting the study region, but future projections of change appeared weak or mixed. The most pronounced anticipated change was a deepening or strengthening (and a possible increase in duration according to GFDL) of storms by 2100. Strengthening of storms has been tied to reduced sea ice coverage [47] but the specific mechanisms for explaining changes in the storm characteristics in the Foggy Island Bay region are uncertain. General trends of Arctic storms in observational data over the historical record are generally mixed by season, region and even the data source/methodology [48]. Trend signals also emerged based on our analysis of the downscaled future projections of sea level pressure, although there was a noteworthy divergence between the future trajectories of GFDL and CCSM. The CCSM simulation does not capture the historical Beaufort High as well as GFDL, and CCSM had more storms per year on average than GFDL or the reanalysis in the overlapping historical period (146 per year in CCSM vs. approximately 131 per year in all others). The CCSM model that was used to generate the data that drove the WRF downscaled simulations for this study had a known bias toward lower sea level pressure over the Arctic [49]. This bias adds uncertainty to the use of the CCSM projection in this study therefore it may be prudent to highlight GFDL when the results diverge. However, as was the case for observational trends in Arctic storminess, the projected trends from the broader range of CMIP5 global climate models and scenarios are generally mixed [48]. A previous analysis of CMIP5 projections from global and regional climate models anticipated a decline in the frequency of cyclones over the Beaufort Sea in winter [50]. This projected winter decline is also apparent when looking across various ensembles of global climate models associated with CMIP3, 5 and 6 (it is even more prominent in CMIP6), while increased storminess is generally anticipated in the summer [51].

The GFDL showed statistically significant anticipated declines in sea level pressure over the Beaufort Sea and Arctic over 2015–2100 in all seasons. This would indicate a decline in the strength of the Beaufort High and therefore an increase in storminess, which would be due to increases in either the duration or strength of storms and not the overall number based on our results. Consistent with our findings, a projected increase in wave-driven erosion along the Beaufort Sea coast by 2081–2100 was found based on wave modeling using five CMIP5 global climate model projections and was similarly attributed to a weakened Beaufort High [52]. These historical and projected changes in storminess related to variability in the strength of the Beaufort High are therefore a key large-scale atmospheric driver of westerly winds and high water events along the coast in the Foggy Island Bay region.

Change in past and future frequency of extreme high water events in Foggy Island Bay is intertwined with change in winds, storms, and sea ice. While westerly winds are projected to increase based on our analysis, sea ice, which is a key secondary driver of events, has declined over the observational record and is anticipated to continue to do so. Besides the anticipated changes in the atmospheric drivers, a rise in relative sea level (SLR) is also anticipated, potentially exasperating coastal impacts and erosion. Climate model-based scenarios suggest a rise in SLR to be between 0.7 and 2 m between 2000 and 2100, albeit linear extrapolation of the current measured trend at the Prudhoe Bay tide gauge ( $3.4 \pm 1.44$  mm/yr from 1988 to 2021) suggests ~25 cm by the year 2100 [53].

In summary, historical wind speeds in the region have experienced a slight increase over the last 2–3 decades based on reanalysis data along with an upward trend in the annual counts of storms, and an increase in open water that resulted in increased ocean wave heights [54]. The frequency of high wind events has also increased over the Beaufort Sea region [21]. Future projections according to a subset of models from CMIP5 indicated that mean and high wind speeds will increase over the Beaufort Sea and at Deadhorse [28]. The seasonality analysis of westerly wind events found that most events occur in Dec-Jan with a minimum during the summer. The frequency of events during the fall and winter is also projected to increase based on our analysis of the downscaled climate models. While sea ice is anticipated to decline during the fall/winter, high water events, including extreme events, were found to occur during the winter months with high sea ice coverage. This is consistent with prior analysis of storm surge flooding along the Beaufort Sea coast [55]. While there is uncertainty in the future frequency of storms in the Beaufort Sea, a possible increase in the strength and/or duration of storms impacting the region may enhance the frequency of westerly winds and high water events in Foggy Island Bay in the coming decades. However, confounding factors that may also impact potential future change in coastal water levels include the role of tides and sea level rise and those were not fully evaluated in this study.

## 5. Conclusions

High water levels in Foggy Island Bay in northern Alaska were found to occur in conjunction with westerly winds. The westerly winds are in contrast to the predominant easterly winds in this area of the Beaufort Sea coast, which are typically driven by the Beaufort High. Westerly winds in Foggy Island Bay are linked with the passage of low pressure storm systems north and east of the region. Historical trends in sea level pressure were generally mixed throughout the year, although there are indications in the literature that the Beaufort High has weakened in the winter months in recent decades. The results also indicated an increase in the annual number of storms impacting the region over the historical period. These factors have resulted in a slight increase in the frequency of days with westerly winds over the 1979–2015 period. The two downscaled climate model projections used in this study on the future frequency of westerly winds and associated sea level pressure from CCSM and GFDL diverge in our analysis. However, the CCSM global climate model contains known biases that increase the uncertainty of its projection over that of GFDL. The downscaled GFDL projections indicate that days with westerly winds will become more frequent over the next ~80 years as storms intensify or impact the region for longer periods and, in conjunction with more open water, may result in more high water events in Foggy Island Bay. While beyond the scope of this study, better understanding the drivers of past and potential future change in storms (number, strength, and duration) impacting northern Alaska could help to constrain the uncertainty in the projections.

The conclusions of this study can be used to inform future development in the region, specifically through the consideration of the vulnerability of coastal areas to inundation and erosion from high water storm events. Evaluation of additional climate models and scenarios, while beyond the scope of this study, could be undertaken in planning efforts to provide a broader range of the uncertainties. Additional coastal wave modeling studies focused on extreme high water events may also be necessary to better refine the interplay

of their ice, ocean, and atmospheric drivers. These more focused modeling studies should also assess the role of tides and sea level rise when evaluating future change in the extremes. As the global climate continues to warm and the Arctic experiences change and new development opportunities, forecasting such storm events will likely become increasingly important. Sustained observations, like the tide gauge at Prudhoe Bay, will be critical to develop such forecasts and monitor for changes into the future.

**Author Contributions:** Conceptualization, P.A.B. and L.E.; methodology, P.A.B.; software, P.A.B.; validation, P.A.B. and L.E.; formal analysis, P.A.B.; investigation, P.A.B.; resources, P.A.B.; data curation, P.A.B.; writing—original draft preparation, P.A.B.; writing—review and editing, L.E. and J.K.; visualization, P.A.B.; supervision, P.A.B.; project administration, J.K.; funding acquisition, J.K. All authors have read and agreed to the published version of the manuscript.

**Funding:** Funding for this research was provided by the U.S. Bureau of Ocean Energy Management (cooperative agreement no. M17AC00020; UAF) and an interagency agreement (grant no. M17PG00046; USGS) for the project titled “Wave and Hydrodynamic Modeling Within the Nearshore Beaufort Sea”.

**Institutional Review Board Statement:** Not applicable.

**Informed Consent Statement:** Not applicable.

**Data Availability Statement:** The dynamically downscaled reanalysis and future projections data utilized in this study are available at <https://registry.opendata.aws/wrf-alaska-snap/> (accessed on 1 August 2018). CBHAR is available at <https://portal.aos.org/> (accessed on 10 August 2018). The water level data is available at <https://tidesandcurrents.noaa.gov/stationhome.html?id=9497645> (accessed on 1 February 2019). Winds at the Deadhorse Airport were obtained from <https://mesonet.agron.iastate.edu/request/download.phtml> (accessed on 15 September 2020) and <http://windtool.accap.uaf.edu/> (accessed on 15 September 2020). The storm track data can be obtained on request from the authors.

**Acknowledgments:** The authors thank Uma Bhatt, Rick Lader, John Walsh, Carol Janzen, Warren Horowitz, Heather Crowley, Tom Ravens, and the two anonymous reviewers for their comments and suggestions that helped to improve this study.

**Conflicts of Interest:** The authors declare no conflict of interest.

## References

1. Bird, K.J.; Charpentier, R.R.; Gautier, D.L.; Houseknecht, D.W.; Klett, T.R.; Pitman, J.K.; Moore, T.E.; Schenk, C.J.; Tennyson, M.E.; Wandrey, C.J. *Circum-Arctic Resource Appraisal: Estimates of Undiscovered Oil and Gas North of the Arctic Circle*; USGS Fact Sheet 2008-3049; U.S. Geological Survey: Reston, VA, USA, 2008; pp. 1–4. [CrossRef]
2. Bekryaev, R.V.; Polyakov, I.V.; Alexeev, V.A. Role of Polar Amplification in Long-Term Surface Air Temperature Variations and Modern Arctic Warming. *J. Clim.* **2010**, *23*, 3888–3906. [CrossRef]
3. Serreze, M.C.; Barry, R.G. Processes and Impacts of Arctic Amplification: A Research Synthesis. *Glob. Planet. Chang.* **2011**, *77*, 85–96. [CrossRef]
4. Terenzi, J.; Jorgenson, M.T.; Ely, C.R. Storm-Surge Flooding on the Yukon-Kuskokwim Delta, Alaska. *Arctic* **2014**, *67*, 360–374. [CrossRef]
5. Sultan, N.J.; Braun, K.W.; Thieman, D.S.; Sampath, A. North Slope Trends in Sea Level, Storm Frequency, Duration and Intensity. In Proceedings of the SNAME 9th International Conference and Exhibition on Performance of Ships and Structures in Ice, Anchorage, AK, USA, 20–23 September 2010.
6. Lantz, T.C.; Moffat, N.D.; Jones, B.M.; Chen, Q.; Tweedie, C.E. Mapping Exposure to Flooding in Three Coastal Communities on the North Slope of Alaska Using Airborne LiDAR. *Coast. Manag.* **2020**, *48*, 96–117. [CrossRef]
7. Lynch, A.H.; Lestak, L.R.; Uotila, P.; Cassano, E.N.; Xie, L. A Factorial Analysis of Storm Surge Flooding in Barrow, Alaska. *Mon. Weather Rev.* **2008**, *136*, 898–912. [CrossRef]
8. Irrgang, A.M.; Lantuit, H.; Manson, G.K.; Günther, F.; Grosse, G.; Overduin, P.P. Variability in Rates of Coastal Change Along the Yukon Coast, 1951 to 2015. *J. Geophys. Res. Earth Surf.* **2018**, *123*, 779–800. [CrossRef]
9. Kowalik, Z. Storm Surges in the Beaufort and Chukchi Seas. *J. Geophys. Res.* **1984**, *89*, 10570. [CrossRef]
10. Reimnitz, E.; Maurer, D.K. Effects of Storm Surges on the Beaufort Sea Coast, Northern Alaska. *Arctic* **1979**, *32*, 329–344. [CrossRef]
11. Kim, J.; Murphy, E.; Nistor, I.; Ferguson, S.; Provan, M. Numerical Analysis of Storm Surges on Canada’s Western Arctic Coastline. *J. Mar. Sci. Eng.* **2021**, *9*, 326. [CrossRef]

12. Walker, D.A.; Webber, P.J. Relationships of Soil Acidity and Air Temperature to the Wind and Vegetation at Prudhoe Bay, Alaska. *Arctic* **1979**, *32*, 224–236. [[CrossRef](#)]
13. Overland, J.E. Meteorology of the Beaufort Sea. *J. Geophys. Res.* **2009**, *114*, C00A07. [[CrossRef](#)]
14. Serreze, M.C.; Barrett, A.P. Characteristics of the Beaufort Sea High. *J. Clim.* **2011**, *24*, 159–182. [[CrossRef](#)]
15. Bieniek, P.A.; Bhatt, U.S.; Walker, D.A.; Raynolds, M.K.; Comiso, J.C.; Epstein, H.E.; Pinzon, J.E.; Tucker, C.J.; Thoman, R.L.; Tran, H.; et al. Climate Drivers Linked to Changing Seasonality of Alaska Coastal Tundra Vegetation Productivity. *Earth Interact.* **2015**, *19*, 1–29. [[CrossRef](#)]
16. Zhang, T.; Osterkamp, T.E.; Stamnes, K. Some Characteristics of the Climate in Northern Alaska, U.S.A. *Arct. Alp. Res.* **1996**, *28*, 509–518. [[CrossRef](#)]
17. Kozo, T.L. Evidence for Sea Breezes on the Alaskan Beaufort Sea Coast. *Geophys. Res. Lett.* **1979**, *6*, 849–852. [[CrossRef](#)]
18. Moritz, R.E. On a Possible Sea-Breeze Circulation near Barrow, Alaska. *Arct. Alp. Res.* **1977**, *9*, 427–431. [[CrossRef](#)]
19. Walsh, J.E. Measurements of the Temperature, Wind, and Moisture Distribution across the Northern Coast of Alaska. *Arct. Alp. Res.* **1977**, *9*, 175–182. [[CrossRef](#)]
20. Kenigson, J.S.; Timmermans, M.L. Arctic Cyclone Activity and the Beaufort High. *J. Clim.* **2021**, *34*, 4119–4127. [[CrossRef](#)]
21. Stegall, S.T.; Zhang, J. Wind Field Climatology, Changes, and Extremes in the Chukchi-Beaufort Seas and Alaska North Slope during 1979–2009. *J. Clim.* **2012**, *25*, 8075–8089. [[CrossRef](#)]
22. Baule, W.J.; Shulski, M.D. Climatology and Trends of Wind Speed in the Beaufort/Chukchi Sea Coastal Region from 1979 to 2009. *Int. J. Climatol.* **2014**, *34*, 2819–2833. [[CrossRef](#)]
23. Rinke, A.; Maturilli, M.; Graham, R.M.; Matthes, H.; Handorf, D.; Cohen, L.; Hudson, S.R.; Moore, J.C. Extreme Cyclone Events in the Arctic: Wintertime Variability and Trends. *Environ. Res. Lett.* **2017**, *12*, 094006. [[CrossRef](#)]
24. Sepp, M.; Jaagus, J. Changes in the Activity and Tracks of Arctic Cyclones. *Clim. Chang.* **2011**, *105*, 577–595. [[CrossRef](#)]
25. Ballinger, T.J.; Walsh, J.E.; Bhatt, U.S.; Bieniek, P.A.; Tschudi, M.A.; Brettschneider, B.; Eicken, H.; Mahoney, A.R.; Richter-Menge, J.; Shapiro, L.H. Unusual West Arctic Storm Activity During Winter 2020: Another Collapse of the Beaufort High? *Geophys. Res. Lett.* **2021**, *48*, e2021GL092518. [[CrossRef](#)]
26. Moore, G.W.K.; Schweiger, A.; Zhang, J.; Steele, M. Collapse of the 2017 Winter Beaufort High: A Response to Thinning Sea Ice? *Geophys. Res. Lett.* **2018**, *45*, 2860–2869. [[CrossRef](#)]
27. Redilla, K.; Pearl, S.T.; Bieniek, P.A.; Walsh, J.E. Wind Climatology for Alaska: Historical and Future. *Atmos. Clim. Sci.* **2019**, *09*, 683–702. [[CrossRef](#)]
28. Basu, S.; Walsh, J.E. Climatological Characteristics of Historical and Future High-Wind Events in Alaska. *Atmos. Clim. Sci.* **2018**, *8*, 373–394. [[CrossRef](#)]
29. Walsh, J.E.; Bhatt, U.S.; Littell, J.S.; Leonawicz, M.; Lindgren, M.; Kurkowski, T.A.; Bieniek, P.A.; Thoman, R.; Gray, S.; Rupp, T.S. Downscaling of Climate Model Output for Alaskan Stakeholders. *Environ. Model. Softw.* **2018**, *110*, 38–51. [[CrossRef](#)]
30. Skamarock, W.C.; Skamarock, W.C.; Klemp, J.B.; Dudhia, J.; Gill, D.O.; Barker, D.M.; Wang, W.; Powers, J.G. *A Description of the Advanced Research WRF Version 3*; NCAR Technical Note -475+STR; National Center for Atmospheric Research: Boulder, CO, USA, 2008.
31. Bieniek, P.A.; Bhatt, U.S.; Walsh, J.E.; Rupp, T.S.; Zhang, J.; Krieger, J.R.; Lader, R. Dynamical Downscaling of ERA-Interim Temperature and Precipitation for Alaska. *J. Appl. Meteorol. Climatol.* **2016**, *55*, 635–654. [[CrossRef](#)]
32. Lader, R.; Walsh, J.E.; Bhatt, U.S.; Bieniek, P.A. Projections of Twenty-First-Century Climate Extremes for Alaska via Dynamical Downscaling and Quantile Mapping. *J. Appl. Meteorol. Climatol.* **2017**, *56*, 2393–2409. [[CrossRef](#)]
33. Lader, R.; Walsh, J.E.; Bhatt, U.S.; Bieniek, P.A. Agro-Climatic Projections for a Warming Alaska. *Earth Interact.* **2018**, *22*, 1–24. [[CrossRef](#)]
34. Morrison, H.; Thompson, G.; Tatarskii, V. Impact of Cloud Microphysics on the Development of Trailing Stratiform Precipitation in a Simulated Squall Line: Comparison of One- and Two-Moment Schemes. *Mon. Weather Rev.* **2009**, *137*, 991–1007. [[CrossRef](#)]
35. Iacono, M.J.; Delamere, J.S.; Mlawer, E.J.; Shephard, M.W.; Clough, S.A.; Collins, W.D. Radiative Forcing by Long-Lived Greenhouse Gases: Calculations with the AER Radiative Transfer Models. *J. Geophys. Res.* **2008**, *113*, 13103. [[CrossRef](#)]
36. Janjić, Z.I. The Step-Mountain Eta Coordinate Model: Further Developments of the Convection, Viscous Sublayer, and Turbulence Closure Schemes. *Mon. Weather Rev.* **1994**, *122*, 927–945. [[CrossRef](#)]
37. Zhang, X.; Walsh, J.E.; Zhang, J.; Bhatt, U.S.; Ikeda, M. Climatology and Interannual Variability of Arctic Cyclone Activity: 1948–2002. *J. Clim.* **2004**, *17*, 2300–2317. [[CrossRef](#)]
38. Liu, F.; Krieger, J.R.; Zhang, J. Toward Producing the Chukchi-Beaufort High-Resolution Atmospheric Reanalysis (CBHAR) via the WRFDA Data Assimilation System. *Mon. Weather Rev.* **2014**, *142*, 788–805. [[CrossRef](#)]
39. Zhang, J.; Liu, F.; Tao, W.; Krieger, J.; Shulski, M.; Zhang, X. Mesoscale Climatology and Variation of Surface Winds over the Chukchi-Beaufort Coastal Areas. *J. Clim.* **2016**, *29*, 2721–2739. [[CrossRef](#)]
40. Lund, I.A. Map-Pattern Classification by Statistical Methods. *J. Appl. Meteorol.* **1963**, *2*, 56–65. [[CrossRef](#)]
41. Dee, D.P.; Uppala, S.M.; Simmons, A.J.; Berrisford, P.; Poli, P.; Kobayashi, S.; Andrae, U.; Balmaseda, M.A.; Balsamo, G.; Bauer, P.; et al. The ERA-Interim Reanalysis: Configuration and Performance of the Data Assimilation System. *Q. J. R. Meteorol. Soc.* **2011**, *137*, 553–597. [[CrossRef](#)]
42. Tilburg, C.E.; Garvine, R.W. A Simple Model for Coastal Sea Level Prediction. *Weather Forecast.* **2004**, *19*, 511–519. [[CrossRef](#)]

43. Danielson, S.L.; Hennon, T.D.; Hedstrom, K.S.; Pnyushkov, A.V.; Polyakov, I.V.; Carmack, E.; Filchuk, K.; Janout, M.; Makhotin, M.; Williams, W.J.; et al. Oceanic Routing of Wind-Sourced Energy Along the Arctic Continental Shelves. *Front. Mar. Sci.* **2020**, *7*, 509. [[CrossRef](#)]
44. Moore, G.W.K.; Pickart, R.S. The Wrangel Island Polynya in Early Summer: Trends and Relationships to Other Polynyas and the Beaufort Sea High. *Geophys. Res. Lett.* **2012**, *39*, L05503. [[CrossRef](#)]
45. Hudak, D.R.; Young, J.M.C. Storm Climatology of the Southern Beaufort Sea. *Atmos. Ocean* **2002**, *40*, 145–158. [[CrossRef](#)]
46. Vessey, A.F.; Hodges, K.I.; Shaffrey, L.C.; Day, J.J. An Inter-Comparison of Arctic Synoptic Scale Storms between Four Global Reanalysis Datasets. *Clim. Dyn.* **2020**, *54*, 2777–2795. [[CrossRef](#)]
47. Valkonen, E.; Cassano, J.; Cassano, E. Arctic Cyclones and Their Interactions With the Declining Sea Ice: A Recent Climatology. *J. Geophys. Res. Atmos.* **2021**, *126*, 1–35. [[CrossRef](#)]
48. Walsh, J.E.; Ballinger, T.J.; Euskirchen, E.S.; Hanna, E.; Mård, J.; Overland, J.E.; Tangen, H.; Vihma, T. Extreme Weather and Climate Events in Northern Areas: A Review. *Earth-Sci. Rev.* **2020**, *209*, 103324. [[CrossRef](#)]
49. De Boer, G.; Chapman, W.; Kay, J.E.; Medeiros, B.; Shupe, M.D.; Vavrus, S.; Walsh, J. A Characterization of the Present-Day Arctic Atmosphere in CCSM4. *J. Clim.* **2012**, *25*, 2676–2695. [[CrossRef](#)]
50. Akperov, M.; Rinke, A.; Mokhov, I.I.; Semenov, V.A.; Parfenova, M.R.; Matthes, H.; Adakudlu, M.; Boberg, F.; Christensen, J.H.; Dembitskaya, M.A.; et al. Future Projections of Cyclone Activity in the Arctic for the 21st Century from Regional Climate Models (Arctic-CORDEX). *Glob. Planet. Chang.* **2019**, *182*, 103005. [[CrossRef](#)]
51. Harvey, B.J.; Cook, P.; Shaffrey, L.C.; Schiemann, R. The Response of the Northern Hemisphere Storm Tracks and Jet Streams to Climate Change in the CMIP3, CMIP5, and CMIP6 Climate Models. *J. Geophys. Res. Atmos.* **2020**, *125*, e2020JD032701. [[CrossRef](#)]
52. Casas-Prat, M.; Wang, X.L. Projections of Extreme Ocean Waves in the Arctic and Potential Implications for Coastal Inundation and Erosion. *J. Geophys. Res. Ocean.* **2020**, *125*, e2019JC015745. [[CrossRef](#)]
53. Sweet, W.V.; Hamlington, B.D.; Kopp, R.E.; Weaver, C.P.; Barnard, P.L.; Bekaert, D.; Brooks, W.; Craghan, M.; Dusek, G.; Frederikse, T.; et al. *Global and Regional Sea Level Rise Scenarios for the United States*; NOAA Tech. Rep. NOS 01 ; National Oceanic and Atmospheric Administration: Silver Spring, MD, USA, 2022; 111p.
54. Nederhoff, K.; Erikson, L.; Engelstad, A.; Bieniek, P.; Kasper, J. The Effect of Changing Sea Ice on Wave Climate Trends along Alaska's Central Beaufort Sea Coast. *Cryosphere* **2022**, *16*, 1609–1629. [[CrossRef](#)]
55. Reimnitz, E.; Maurer, D.K. *Storm Surges in the Alaskan Beaufort Sea*; US Geological Survey: Reston, VA, USA, 1978; Volume 78.